1-2009

Phase Diagrams of Binary Alloys Calculated from a Density Functional Theory

Vadim B. Warshavsky
Iowa State University

Xueyu Song
Iowa State University, xsong@iastate.edu

Phase Diagrams of Binary Alloys Calculated from a Density Functional Theory

Abstract
Phase behaviors of binary alloys with an embedded atom model potential are investigated using the thermodynamic perturbation theory. The free energies of the liquid and solid phases are computed using the fundamental measure density functional theory and accurate approximations to the hard-sphere mixture correlation functions. The method is applied to calculate the Au-Cu alloy phase diagram. To improve the accuracy of the computed phase diagram, we developed a systematic approach to optimize the model potential of Au-Cu by adjusting the melting temperature of the pure Au to its experimental one. With such an optimized potential the computed Au-Cu alloy phase diagram is in good agreement with the experimental one for the whole composition range.

Disciplines
Chemistry

Comments
This article is from *Physical Review B* 79 (2009): 015101, doi:10.1103/PhysRevB.79.014101. Posted with permission.

Phase diagrams of binary alloys calculated from a density functional theory

Vadim B. Warshavsky and Xueyu Song
Department of Chemistry and Ames Laboratory, Iowa State University, Ames, Iowa 50011, USA
(Received 7 October 2008; revised manuscript received 11 November 2008; published 5 January 2009)

Phase behaviors of binary alloys with an embedded atom model potential are investigated using the thermodynamic perturbation theory. The free energies of the liquid and solid phases are computed using the fundamental measure density functional theory and accurate approximations to the hard-sphere mixture correlation functions. The method is applied to calculate the Au-Cu alloy phase diagram. To improve the accuracy of the computed phase diagram, we developed a systematic approach to optimize the model potential of Au-Cu by adjusting the melting temperature of the pure Au to its experimental one. With such an optimized potential the computed Au-Cu alloy phase diagram is in good agreement with the experimental one for the whole composition range.

DOI: 10.1103/PhysRevB.79.014101 PACS number(s): 64.10.+h, 64.75.−g

I. INTRODUCTION

In this paper a method based on the thermodynamic perturbation theory and density functional theory (DFT) is applied to compute free energies of liquid and solid mixtures and, hence, to study alloy phase behaviors. In the framework of the Weeks, Chandler, and Andersen (WCA) perturbation theory for liquids and solids,[1–3] a pair intermolecular potential is split into a reference part and a perturbative one; the former is mapped onto an effective hard-sphere (HS) system. The free energy is, thus, separated into two parts: one of them is the free energy of HS reference system, whereas the second one is the perturbation. The latter can be obtained from the perturbative potential and the correlation functions of the HS system. We note that a similar strategy has been used before[4–7] although the calculations of free energies of binary liquid and solid alloys at these studies were based on the different methodologies rather than on a single theoretical approach. Our strategy to compute liquid and solid thermodynamic properties within the same theoretical framework provides an important advantage for a consistent description of solid-liquid phase coexistence.

Previously, the WCA perturbation theory has been applied to calculate free energies of single-component metallic[8] and Lennard-Jones (LJ) (Ref. 9) liquids and solids to study the freezing of pure liquids. In Ref. 8 the parameters of the reference HS systems were taken from simulations, whereas in Ref. 9 the necessary properties of the HS system were obtained from the fundamental measure (FM) DFT.[10–12] Such a self-contained theoretical approach without requiring any inputs from simulations is especially useful for multicomponent systems because simulation results sometimes are not easily accessible.

The theories for HS *liquid* mixtures were proposed before to calculate free energies[13,14] and correlation functions.[15] Such studies made possible for the applications of the thermodynamical perturbation theory to liquid mixtures.[16] Recently we developed a theoretical method to compute the correlation functions of HS solid mixtures.[17] Combined with the DFT for solids[18–21] this method allows us to calculate free energies of solid mixtures with realistic interaction potentials and, hence, to study the phase behaviors of realistic molecular mixtures. An application to the freezing of LJ mixtures[22] has been successful as the obtained spindle- and azeotropic-type solid-liquid phase diagrams of LJ mixtures are in good agreement with the corresponding ones from simulations.

In the present paper this methodology is applied to study the freezing of liquid Au-Cu alloy with an embedded atom model (EAM).[23] In general, EAM model potentials are widely used to describe many properties of metals and alloys.[24,25] These potentials have a density-dependent term, which includes many-body interactions. As any theoretical calculations based on the perturbation theory, a pair potential is needed. Previously, Foiles[26] proposed a method to extract a density-dependent effective pair potential of an EAM potential of pure metals. Here we generalize this method to alloys. Typically the model metallic interaction potentials are optimized with respect to the experimental mechanical properties of an alloy. The nonmechanical properties, such as the melting temperature, are not necessarily reproduced and may deviate significantly from the experimental one. For example, there is a significant difference in the melting temperature for pure Au from the comparison between the experimental one and the one from simulations[27] using the EAM model of Au-Cu alloy.[23] Thus there is a great interest to incorporate some experimental thermodynamic properties into the development of model potentials. But such a program is very time consuming in general if using computer simulations.[28] In this paper we show that a Gibbs-Duhem integration method can be used to optimize the EAM model potential[28] such that the Au melting temperature is in close agreement with its experimental value. With such an improved potential we obtained a solid-liquid phase diagram of Au-Cu mixture to be in good agreement with the experimental one for the whole composition range. Thus our work indicates that it is possible to compute phase diagrams of alloys accurately and reliably from DFT and the WCA perturbation theory. Furthermore, such a methodology can also be used to incorporate thermodynamic properties of metallic systems into the development of model potentials without invoking the computationally intensive molecular simulations.

The rest of the paper is organized as follows. In Sec. II we outline the theoretical methods used to calculate the effective

pair potentials and free energies of alloys. In Sec. III we present a solid-liquid phase diagram of Au-Cu alloy and compare it with the experimental one. Then we discuss a method to reparametrize the EAM model potential of Au-Cu using Au experimental melting temperature as an input. Some concluding remarks are given in Sec. IV.

II. THEORY

Consider an alloy with an EAM. Within this model the total energy E_{tot} of a metallic system is given by[24]

$$E_{\text{tot}} = \sum_k U_i(e_k) + \frac{1}{2}\sum_{k\neq m} \phi_{ij}(r_{km}), \tag{1}$$

$$e_k = \sum_{k\neq m} f_j(r_{km}), \tag{2}$$

where U_i is the energy for an embedding atom-type i when the electron density is e_k at position $\vec{r}_k$ and ϕ_{ij} is the repulsive pair interaction between atom types of i and j located at $\vec{r}_k$ and $\vec{r}_m$, respectively. The term $f_j(r_{km})$ is the contribution of atom-type j at $\vec{r}_m$ to the electron density at $\vec{r}_k$ and $r_{km}=|\vec{r}_k-\vec{r}_m|$. The summations run over all atoms in the system.

Foiles[26] proposed a method, which is based on the expansion around the average electron density, to approximate the many-body interaction in Eq. (1) by an effective density-dependent pair potential. This method is known to be able to give accurate thermodynamic and structural properties.[8,26] A straightforward generalization of this method to binary mixtures gives us the following total energy,

$$E_{\text{tot}} = \sum_{i=1}^{2} N_i[U_i(\bar{e}) - \bar{e}U_i'(\bar{e})] + \frac{1}{2}\sum_{k\neq m} \psi_{ij}(r_{km}), \tag{3}$$

where N_i is the number of atoms of i type and $\psi_{ij}(r)$ is an effective pair potential;

$$\psi_{ij}(r) = \phi_{ij}(r) + U_j'(\bar{e})f_i(r) + U_i'(\bar{e})f_j(r) + \frac{1}{2}U_j''(\bar{e})[f_i(r)]^2 + \frac{1}{2}U_i''(\bar{e})[f_j(r)]^2. \tag{4}$$

In the above expressions the symbols $'$ and $''$ denote the first and second derivatives with respect to the electron density. For practical calculations of the average host electron density $\bar{e}$, we generalize the Foiles prescription and approximate it by the average electron density for substitutionally disordered fcc solid solution with a lattice constant such that the overall atomic density matches a given bulk density.

In the present study we consider an fcc Au-Cu solid solution. It is known that EAM potentials work well for fcc structure[29] and the applicability of Eqs. (3) and (4) together with the definition of the average electron density for other lattices (for instance, bcc) still need to be tested.[30]

To calculate the free energies of liquid and solid phases using the WCA perturbation theory, the potentials $\psi_{ij}(r)$ are separated into a short-range, purely repulsive reference part $\psi_{ij}^{(\text{ref})}(r)$ and a perturbative part $\psi_{ij}^{(\text{pert})}(r)$; the reference system is mapped onto an effective HS system with a set of temperature-dependent HS diameters $\{d_{ij}\}$ [with $d_{11}<d_{22}$ and $d_{12}=(d_{11}+d_{22})/2$] prescribed by the WCA criteria for mixtures.[16,22,31] Using Eq. (3) the resulting expression for the total Helmholtz free energy is

$$F(x,\rho,T) = N\sum_{i=1}^{2} x_i[U_i(\bar{e}) - \bar{e}U_i'(\bar{e})] + F_{\text{HS}} + \frac{N\rho}{2}\sum_{i,j=1}^{2} x_i x_j \int d\vec{r} g_{ij}^{(\text{HS})}(r)\psi_{ij}^{(\text{pert})}(r), \tag{5}$$

where T is the temperature, N is the total number of particles, ρ is the total density, x_i is the molar fraction of type i particles, and F_{HS} and $g_{ij}^{(\text{HS})}(r)$ are the free energy and correlation functions, respectively, of the HS reference system. The latter is characterized by the total packing fraction $\eta=\frac{\pi}{6}\rho(x_1 d_{11}^3+x_2 d_{22}^3)$, the molar fraction of larger spheres $x=x_2$, and the diameters ratio $\delta=d_{11}/d_{22}$.

To calculate the free energy F_{HS} of an HS system we use the classical DFT.[32] The DFT approach is based on the existence of a functional $F_{\text{HS}}[\rho_1(\vec{r}),\rho_2(\vec{r})]$ of the densities of particles of each species. In practice F_{HS} is split into an (exactly known) ideal gas contribution F_{id} and an excess contribution F_{ex}, the latter depending entirely upon interparticle interactions. We approximate the excess functional F_{ex} by a fundamental measure density functional,[11,12]

$$F_{\text{ex}} = \int d\vec{r}\Phi\{n_\alpha(\vec{r})\}, \tag{6}$$

where $\{n_\alpha(\vec{r})\}$ are the weighted densities,

$$n_\alpha(\vec{r}) = \sum_{i=1}^{2}\int d\vec{r}'\rho_i(\vec{r}')\omega_i^{(\alpha)}(\vec{r}-\vec{r}') \tag{7}$$

and $\omega_i^{(\alpha)}$ are the scalar, vector, and tensor weight functions.

Practical calculations require specifying the density distribution and the lattice structure of the crystal. We consider the substitutionally disordered fcc solid solution (this is the case for Au-Cu alloy) with the local densities $\{\rho_i(\vec{r})\}$ being modeled by the Gaussian distributions with width parameters α_1 and α_2. Minimization of the functional F_{HS} with respect to α_1 and α_2 for fixed mixture parameters gives equilibrium values of α_1 and α_2 as well as the HS solid free energy F_{HS}. For a homogeneous HS liquid mixture the functional Eq. (6) reduces to the Boublik-Mansouri-Carnahan-Starling-Leland (BMCSL) expression for the free energy of HS liquid mixtures.[13,14]

For the correlation functions $g_{ij}^{(\text{HS})}(r)$ of an HS solid mixture used in the perturbation theory [Eq. (5)], we generalized a theory of Ref. 33 for single component systems to HS solid mixtures. Within our theory[17] the correlation functions $g_{ij}^{(\text{HS})}(r)$ are defined as a orientational average of two-body densities and are expressed as a sum over coordination shells in such a way that the distributions of the second and higher coordination shells can be approximated in a mean-field fashion and the first shell distribution is parametrized to incorporate the nearest-neighbor correlations. The seven parameters of the first peaks are determined by imposing sum rules to specify the contact values $g_{ij}^{(\text{HS})}(d_{ij})$, the normaliza-

TABLE I. Parameters of the potential model for Au-Cu alloys (Ref. 23).

i/j	B_{ij}	σ_{ij}^r (Å)	A_i	σ_i^e (Å)	C_i (eV)
Cu	7076.56	0.241 535	188.542	0.536 562	1
Au	14 759.9	0.272 639	4162.93	0.366 085	1.421 97
Cu/Au	10 153.2	0.258 268			

tion to the nearest-neighbor number, and the mean distance to nearest neighbors. For a set of given parameters of an HS mixture η, x, and δ and a given solid lattice structure, the FM DFT yields the values of α_1, α_2, pressure P, and derivative $\frac{\partial}{\partial\delta}(\frac{\beta F_{\rm ex}}{N})$, which are combined to determine $g_{ij}^{\rm (HS)}(r)$. The correlation functions are shown to be accurate for moderately asymmetric solid mixtures, i.e., for $\delta \geq 0.90$.[17]

The correlation functions of the HS liquid mixtures $g_{ij}^{\rm (HS)}(r)$ are obtained from the equilibrium condition,[32]

$$\frac{\delta\Omega_{\rm HS}[\rho_{1j}(r),\rho_{2j}(r)]}{\delta\rho_{ij}(r)} = 0 \quad (i=1,2), \tag{8}$$

where

$$\Omega_{\rm HS} = F_{\rm HS} - \sum_{i=1}^{2} \int d\vec{r}\rho_{ij}(\vec{r})[\mu_i - \psi_{ij}^{\rm (HS)}(\vec{r})]$$

is the grand canonical potential functional, $\psi_{ij}^{\rm (HS)}(\vec{r})$ is the HS potential of interaction, $\rho_{ij}(\vec{r})$ is the density profile of i-type particle in an external field of the fixed j-type particle, and μ_i is the chemical potential of i-type particles (computed from the BMCSL equation of state). Again we approximate $F_{\rm HS}$ by the FM density functional and solve the integral equations [Eq. (8)] for $\rho_{1j}(r)$ and $\rho_{2j}(r)$ numerically.[22,34] This procedure is repeated for $j=1,2$ to obtain a set of $\{\rho_{ij}(\vec{r})\}$. The correlation functions are given by the following relation:[35]

$$g_{ij}^{\rm (HS)}(r) = \rho_{ij}(r)/\rho_i. \tag{9}$$

Thus, using the free energies $F_{\rm HS}$ and correlations functions $g_{ij}^{\rm (HS)}(r)$ for HS solid and liquid binary mixtures, we are able to calculate the total Helmholtz free energy $F(x,\rho,T)$ of liquid and solid alloys [Eq. (5)]. To find the coexistence conditions between the liquid and solid phases for a given pressure P and temperature T, we calculate the dependence of liquid and solid Gibbs free energies per particle $G(x,P,T)/N$ on the composition x,

$$\frac{G(x,P,T)}{N} = \frac{F(x,\rho,T)}{N} + \frac{P}{\rho}, \tag{10}$$

where the dependence of the total density ρ on the right-hand side of this formula on the variables x, P, and T can be found from the solution of the equation $P=\rho^2\frac{\partial}{\partial\rho}[\frac{F(x,\rho,T)}{N}]_{x,T}$. The Maxwell double-tangent construction will lead to the desired phase diagram.[22]

In practical applications the enthalpy $H=U+PV$ of metallic alloys is important. As $U_{\rm HS}^{\rm (ex)}=0$ we calculate H per particle using the formula,

$$\frac{H}{N} = \frac{F_{\rm EAM}}{N} + \frac{3}{2}k_BT + \frac{F_{\rm pert}}{N} + \frac{P}{\rho}, \tag{11}$$

where $F_{\rm EAM}$ and $F_{\rm pert}$ are the first and the third term on the right-hand side of Eq. (5).

III. RESULTS

As an illustration of the above method, solid-liquid phase equilibria of an Au-Cu EAM model alloy are calculated. For a particular Au-Cu EAM model the electron densities, the repulsive potential, and the embedding energy are represented as

$$f_i(r) = A_i \exp(-r/\sigma_i^e), \quad \phi_{ij}(r) = B_{ij}\exp(-r/\sigma_{ij}^r),$$
$$U_i(e) = -C_i\sqrt{e}. \tag{12}$$

The model parameters are listed in Table I.

In Figs. 1 and 2 we show the dependence of number density ρ and the enthalpy per particle H/N on the temperature T of liquid Au-Cu alloys for some selected compositions. It is seen that the dependence of ρ and H/N on T is linear and the results of the theoretical calculations agree well with the ones from computer simulations.[27] It is also seen from Fig. 2 that although the enthalpy H/N difference between the theory and simulations is typically couple of percents (for pure Cu the difference is less than 4%), the slopes of H/N curves obtained from the theory and simulations for a given composition have larger deviations. In Fig. 3 we show the

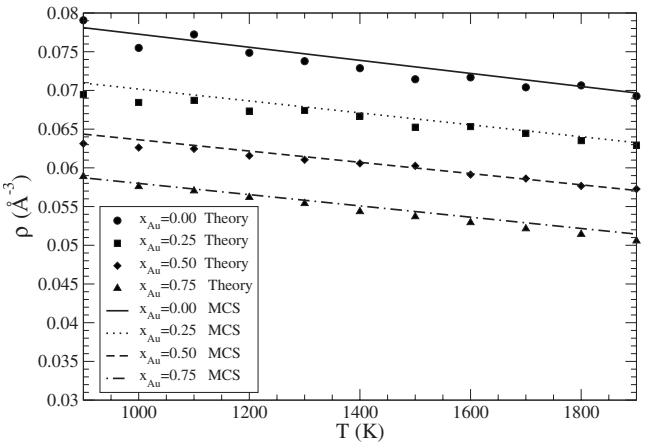

FIG. 1. The dependence of number density $\rho(\text{Å}^{-3})$ on the temperature $T(K)$ for liquid Au-Cu alloys with $x_{\rm Au}=0$, 0.25, 0.5, and 0.75 and $P=1$ atm. The results of the theory are compared with the ones from computer simulations (Ref. 27).

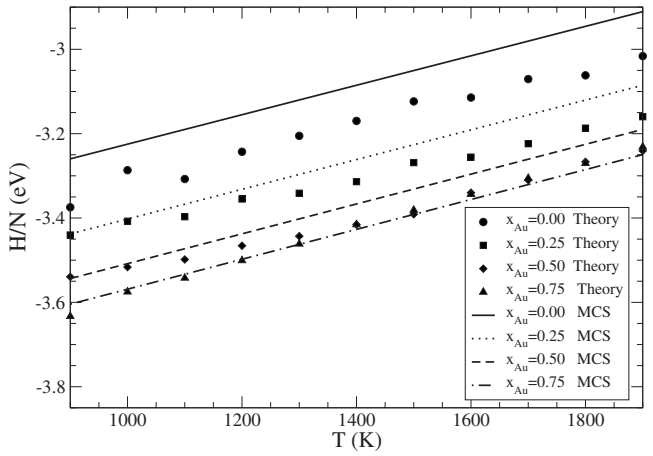

FIG. 2. The dependence of enthalpy per particle H/N(eV) on the temperature $T(K)$ for liquid Au-Cu alloys with $x_{\mathrm{Au}}=0$, 0.25, 0.5, 0.75, and $P=1$ atm. The results of the theory are compared with the ones from computer simulations (Ref. 27).

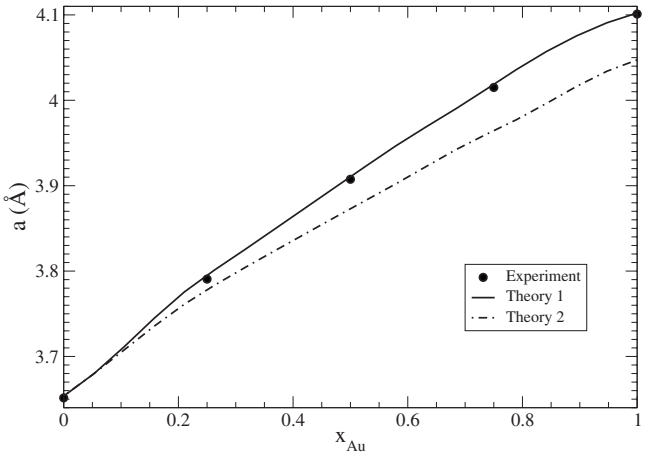

FIG. 4. The dependence of the lattice spacing a(Å) on the composition of solid Au-Cu alloy ($P=1$ atm and $T=748$ K). The results of the theory with the original (Ref. 23) (curve theory 1) and reparametrized (curve theory 2) potential are compared with the experimental one (Ref. 37).

dependence of the specific heat $c_p=\frac{d}{dT}(\frac{H}{N})$ of liquid Au-Cu alloys, which is the slope of a linear $H-T$ dependence, against the composition (curve "theory 1"). It is seen that c_p-T dependence is a decreasing function with a wide plateau region around $x=0.45-0.75$, where the $c_p(T)$ function is almost flat; the difference between the specific heat c_p obtained from the theory and numerical experiments reaches 20% for some compositions, which reflect the difficulty to calculate the derivatives of thermodynamic properties using the perturbation theory.

In Fig. 4 we show the dependence of lattice spacing $a=(4/\rho)^{1/3}$ for the fcc lattice on the composition for $T=748$ K (curve theory 1). It is seen that the theoretical calculations agree well with the experimental ones.

Figure 5 shows a phase diagram for the Au-Cu mixture system (curve theory 1) along with the experimental result.[37] We obtained an azeotrope phase diagram similar to the experimental one. The discrepancy between the results of the theory and experiment is mostly due to the fact that the EAM potential model of Ref. 23 is not quite accurate to reproduce the experimental melting temperature $T_m=1336$ K of pure Au (see Fig. 5). The reason is that the melting temperature is a nonmechanical value, and it is not generally included in the potential development, hence, good agreements of such a quantity with experiment is not necessarily guaranteed. As we can calculate any thermodynamic properties of a model system within our theoretical methodology efficiently, the original EAM model potential can be optimized by adjusting the computed melting temperature of Au to be in agreement with the experimental one using the Gibbs-Duhem integration method.[28,38] For a single-component system a change in each of the parameters $\{X_i\}$ of the potential alters the melting temperature

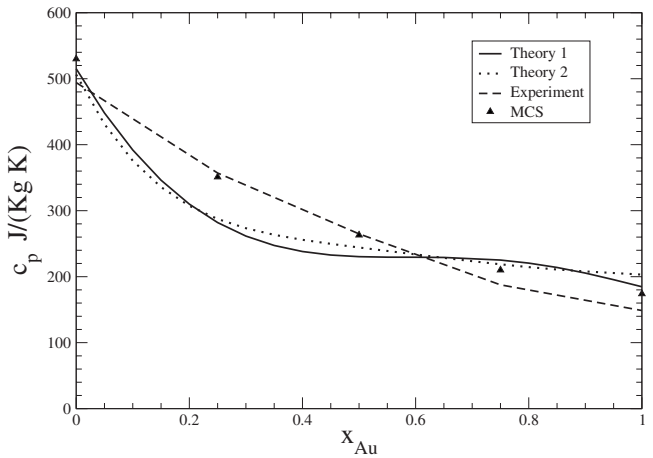

FIG. 3. Specific heat of liquid Au-Cu alloys. The results of the theory with the original (Ref. 23) (curve theory 1) and reparametrized (curve theory 2) potential are compared with the experiment (Ref. 36) and simulation ones (Ref. 27).

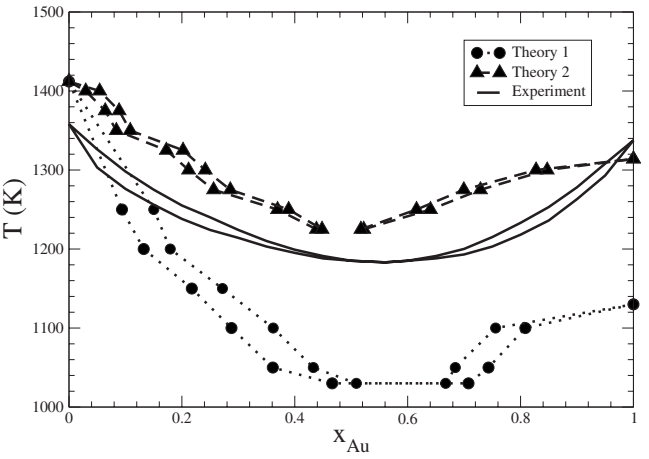

FIG. 5. Temperature-composition (T-x) liquid-solid phase diagrams for the binary Au-Cu system at $P=1$ atm. The results of the theory with the original potential (curve theory 1) and reparametrized (curve theory 2) potential are compared with the experimental one (Ref. 37). The lines to connect the data points are a guide for the eyes only.

TABLE II. The parameters of the coexistence of the liquid and solid Au-Cu mixture systems for various temperatures T: liquid and solid compositions x_l and x_s and number densities ρ_l and ρ_s; the parameters of reference liquid and solid HS systems at the coexistence: the packing fractions η_l and η_s and the diameter ratios δ_l and δ_s.

T (K)	x_l	x_s	ρ_l (Å^{-3})	ρ_s (Å^{-3})	η_l	η_s	δ_l	δ_s
1400	0.0297	0.0543	0.0732	0.0764	0.49	0.52	0.93	0.94
1375	0.0642	0.0888	0.0727	0.0758	0.49	0.52	0.93	0.94
1350	0.0839	0.1085	0.0725	0.0756	0.49	0.53	0.93	0.94
1325	0.1725	0.2021	0.0708	0.0741	0.49	0.53	0.92	0.94
1300	0.2119	0.2415	0.0701	0.0735	0.50	0.53	0.92	0.94
1275	0.2562	0.2858	0.0692	0.0727	0.50	0.54	0.92	0.94
1250	0.3695	0.3892	0.0671	0.0709	0.50	0.54	0.92	0.93
1225	0.4384	0.4483	0.0658	0.0698	0.51	0.54	0.91	0.93
1225	0.5222	0.5172	0.0641	0.0684	0.51	0.54	0.91	0.93
1250	0.6404	0.6157	0.0613	0.0663	0.50	0.54	0.91	0.92
1275	0.7290	0.6995	0.0592	0.0645	0.49	0.54	0.91	0.92
1300	0.8472	0.8275	0.0564	0.0618	0.47	0.55	0.91	0.91

$$T_m(\{X_i\}) = T_{m,0} + \sum_i \left(\frac{\partial T}{\partial X_i}\right)_{X_{j\neq i,0}} (X_i - X_{i,0}), \qquad (13)$$

where $T_{m,0}$ is the melting point of the original model with parameters $\{X_{i,0}\}$. The derivatives at the right-hand side of this equation can be found from the following relation:

$$\left(\frac{\partial T}{\partial X_i}\right)_{P,X_{j\neq i};\text{coex}} = \frac{T(\lambda_{s,i} - \lambda_{l,i})}{(H_s - H_l)}, \qquad (14)$$

where H is the enthalpy and $\lambda_i \equiv (\frac{\partial G}{\partial X_i})_{T,P,X_{j\neq i}}$.

We have calculated $\partial T_m / \partial X_i$ for each of the parameters of pure Au potential from Table I. It was determined that the parameter C_{Au} is mostly responsible for the change in the melting point. We found that the new $C_{\text{Au}} = 1.567\,49$ eV led to the Au experimental melting temperature. Using this new potential we have recalculated the Au-Cu phase diagram shown in Fig. 5 (curve "theory 2"). It is seen that in contrast to the original potential, the new potential model yields a phase diagram, which is in good agreement (within 6%) with the experimental one for the whole composition range. It is also seen from Fig. 5 that for both potentials the theory provides the solidus and liquidus lines to be convex for compositions larger than the azeotropic point, i.e., have qualitatively different behavior compared to experiment. This may be due to the deficiencies of the used perturbation theory[22] or specific functional form of the EAM potential in Eq. (7). Thus, computer simulations of the whole phase diagram may be needed to completely validate the theoretical prediction.

In Table II we assembled the parameters of coexisting solid and liquid phases of Au-Cu alloy with reparametrized potential for some selected temperatures as well as the parameters η and δ of the reference HS systems. The perturbation theory for solid mixtures is accurate if the parameters of the reference HS mixture are in the range of $\delta_s \geq 0.90$ and $\eta_s \leq 0.55$ (Refs. 17 and 22); it is seen that these conditions are always satisfied in this paper. We note that the present result is in qualitative agreement with the empirical Hume-Rothery rule[39] according to which disordered metallic alloys are still stable when the atomic size ratio is larger than 0.85.

The Au-Cu potential was originally developed to fit some experimental properties of solid and liquid Au-Cu alloys. For the new value of the potential parameter C_{Au} we have recalculated a variety of physical properties of these alloys.

In Fig. 6 we show the dependence of number density ρ on the temperature T for pure liquid Au. It is seen that the results for ρ from the reparametrized model agrees a bit better with the experimental data,[37] compared to the ones from our theory and simulations[27] using the original model.

We have also calculated the elastic constants of pure Au for $T=0$. To this end we computed the values of $\partial^2 F / \partial \epsilon_i^2$, where ϵ_i $(i=1,2,3)$ are the parameters of the lattice distortion (we used the fact that for $T=0$ the free energy F is equal to E_{tot} [Eq. (3)]). The connection between the elastic con-

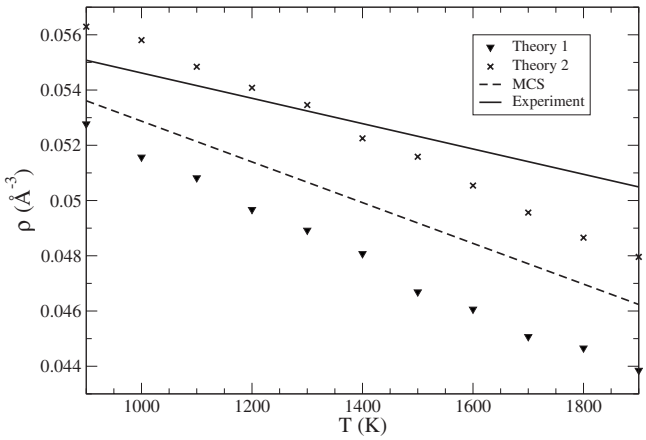

FIG. 6. The dependence of the number density $\rho(\text{Å}^{-3})$ on the temperature $T(K)$ for pure liquid Au. The results of the theory with the original (curve theory 1) and reparametrized (curve theory 2) potential are compared with Monte Carlo simulations (MCS) (Ref. 27) and experiment (Refs. 40 and 41).

TABLE III. The elastic constants C_{11}, C_{12}, and C_{44} and the latent heat of Au obtained from the original version of the EAM potential, the modified version and from the experiment (Refs. 45 and 46) (elastic constants are computed at $T=0$).

	Original	Modified	Experiment
C_{11} (eV/Å^3)	1.28	1.53	1.26
C_{12} (eV/Å^3)	0.99	1.19	1.06
C_{44} (eV/Å^3)	0.38	0.46	0.28
Latent heat (eV/N)	0.19	0.21	0.13

stants and the values of $\partial^2 F/\partial \epsilon_i^2$ for the different types of distortions can be found in Refs. 42–44. We observed that in comparison to the original potential the new potential is slightly worse to model the experimental values of the elastic constants[45] although it still provides these values to be in the reasonable agreement with the experimental ones (Table III). Table III also shows the latent heat of fusion $(=H_l/N - H_s/N)$ of pure Au, which gets slightly worse for the reparametrized potential.

In Fig. 3 we show the dependence of the specific heat $c_p=\frac{d}{dT}(\frac{H}{N})$ against the composition for reparametrized potential (curve theory 2). It is seen that although the result from the reparametrized model differs only slightly from the result of the original model, the specific heat c_p in reparametrized model is a pure decreasing function of the temperature T, the same as it is from the numerical simulations. Therefore we conclude that the model with reparametrized potential is more reasonable to calculate c_p-T dependence compared to the one with the original potential.

In Fig. 4 we show the dependence of lattice spacing a vs composition for reparametrized potential (curve theory 2). It is seen that the difference between the results from the reparametrized and original model is small (the maximum difference is less than 1.3% for pure Au). Both the models and the experiment show the deviation from Vegard's law (the linear dependence between the lattice spacings and compositions for a constant temperature), which is common for many metallic alloys. Previously it was found that along solid-liquid coexistence of HS mixtures the dependence of lattice spacing on composition deviates from linear law when HS diameter ratios are less than 0.90 (the pressure in that study varies with the coexistence curve).[47] For Au-Cu solid mixtures the diameter ratios of reference HS system are from 0.91 to 0.96 along the both theoretical curves in Fig. 4, i.e., it seems that for metallic alloys the form of relationship is also sensitive to other factors rather than just atom size ratio. We note that, naturally, a multiparameter optimization of the potential may be needed to yield perfect agreement for the phase diagram and also other properties of liquid and solid alloys obtained from the theory and experiments.

IV. CONCLUSIONS

To summarize, working with an EAM model, we have implemented a consistent form of thermodynamic perturbation theory, which has comparable accuracy for both the liquid and solid metallic phases, and used it to study the freezing of alloys. We found that the difference in the Au-Cu solid-liquid phase diagrams obtained from the theory and experiment is mostly due to the specific EAM model interaction potential for Au-Cu mixture. A reparametrized EAM model potential for Au-Cu mixture is obtained by adjusting the melting temperature of pure Au to reproduce the experimental value. The computed Au-Cu solid-liquid phase diagram with the new EAM potential is now in good agreement with the experimental one. We note that previously the optimization of an EAM model potential to adjust the melting point was performed using computer simulations,[28] which is a very time-consuming process. We show that the strategy for optimizing potentials using thermodynamic properties can also be achieved efficiently by using the thermodynamical perturbation theory.

We found that the asymmetry of the reference HS mixture along the solid-liquid azeotropic phase diagram for Au-Cu is not very high, with typical values of the diameter ratio of $0.91 \leq \delta \leq 0.94$. It will be interesting to apply the theory to binary alloys where there are larger disparities between HS diameters, for instance, for alloys with eutectic type of phase diagrams, such as Zr-Cu alloy, and also for alloys with other crystal lattices.

Our approach can be extended to study the freezing of ternary liquid alloys because all the involved theories (WCA perturbation theory, FM DFT, the Foiles approach to the effective pair potential, and the methods for HS solid and liquid correlation functions) can be straightforwardly generalized to such multicomponent mixtures. Since within our approach the solid and liquid alloys are treated within a single theoretical framework, it becomes possible to apply this approach to examine also the interface between solid and liquid metallic alloys.[48]

ACKNOWLEDGMENTS

This research was sponsored by the Division of Materials Sciences and Engineering, Office of Basic Energy Sciences, (U.S.) Department of Energy under Contract No. W-7405-ENG-82 with Iowa State University (V.B.W. and X.S.) and by a PRF Grant No. 46451AC6 (X.S.).

[1] J. D. Weeks, D. Chandler, and H. C. Andersen, J. Chem. Phys. **54**, 5237 (1971).
[2] Y. Choi, T. Ree, and F. Ree, J. Chem. Phys. **95**, 7548 (1991).
[3] C. Rascon, L. Mederos, and G. Navascues, Phys. Rev. Lett. **77**, 2249 (1996).
[4] M. Hasegawa and W. H. Young, J. Phys. F: Metal. Phys. **7**, 2271 (1977).
[5] A. I. Landa, V. E. Panin, and M. F. Zhorovkov, Phys. Status

Solidi B **108**, 113 (1981).
[6] J. Hafner, Phys. Rev. B **28**, 1734 (1983).
[7] Z. A. Gurskiy and V. I. Varanitskiy, Fiz. Met. Metalloved. **57**, 883 (1984).
[8] J. R. Morris and X. Song, J. Chem. Phys. **119**, 3920 (2003).
[9] V. B. Warshavsky and X. Song, Phys. Rev. E **69**, 061113 (2004).
[10] Y. Rosenfeld, Phys. Rev. Lett. **63**, 980 (1989).
[11] R. Roth, R. Evans, A. Lang, and G. Kahl, J. Phys.: Condens. Matter **14**, 12063 (2002).
[12] P. Tarazona, Physica A **306**, 243 (2002).
[13] G. A. Mansoori, N. F. Carnahan, K. E. Starling, and T. W. Leland, Jr., J. Chem. Phys. **54**, 1523 (1971).
[14] T. Boublik, J. Chem. Phys. **53**, 471 (1970).
[15] E. W. Grundke and D. Henderson, Mol. Phys. **24**, 269 (1972).
[16] L. L. Lee and D. Levesque, Mol. Phys. **26**, 1351 (1973).
[17] V. B. Warshavsky and X. Song, Phys. Rev. E **77**, 051106 (2008).
[18] J. L. Barrat, M. Baus, and J. P. Hansen, J. Phys. C **20**, 1413 (1987).
[19] S. W. Rick and A. D. J. Haymet, J. Phys. Chem. **94**, 5212 (1990).
[20] X. C. Zeng and D. W. Oxtoby, J. Chem. Phys. **93**, 4357 (1990).
[21] A. R. Denton and N. W. Ashcroft, Phys. Rev. A **42**, 7312 (1990).
[22] V. B. Warshavsky and X. Song, J. Chem. Phys. **129**, 034506 (2008).
[23] G. D. Barrera, R. H. de Tendler, and E. P. Isoardi, Model. Simul. Mater. Sci. Eng. **8**, 389 (2000).
[24] M. S. Daw and M. I. Baskes, Phys. Rev. B **29**, 6443 (1984).
[25] M. S. Daw and M. I. Baskes, Phys. Rev. Lett. **50**, 1285 (1983).
[26] S. M. Foiles, Phys. Rev. B **32**, 3409 (1985).
[27] X. J. Han, M. Chen, and Z. Y. Guo, J. Phys.: Condens. Matter **16**, 705 (2004).
[28] J. B. Sturgeon and B. B. Laird, Phys. Rev. B **62**, 14720 (2000).
[29] J. B. Adams and S. M. Foiles, Phys. Rev. B **41**, 3316 (1990).
[30] J. R. Morris, R. S. Aga, V. Levashov, and T. Egami, Phys. Rev. B **77**, 174201 (2008).
[31] G. Kahl and J. Hafner, J. Phys. F: Met. Phys. **15**, 1627 (1985).
[32] R. Evans, in *Fundamentals of Inhomogeneous Fluid*, edited by D. Henderson (Wiley, New York, 1992).
[33] C. Rascon, L. Mederos, and G. Navascues, Phys. Rev. E **54**, 1261 (1996).
[34] Y. Yu and J. Wu, J. Chem. Phys. **117**, 10156 (2002).
[35] J. K. Percus, in *The Equilibrium Theory of Classical Fluids*, edited by H. L. Frisch and J. L. Lebowitz, (Benjamin, New York, 1964), p. II33.
[36] A. Bykov and E. Pastukhov, J. Therm Anal. Calorim. **60**, 845 (2000).
[37] C. J. Smithells, in *Smithells Metals Reference Book*, edited by E. A. Brandes and G. B. Brook (Butterworths-Heinemann, Oxford, 1992).
[38] D. A. Kofke, Mol. Phys. **78**, 1331 (1993).
[39] W. Hume-Rothery, R. E. Smallman, and C. W. Hayworth, *The Structure of Metals and Alloys* (The Metals and Metalurgy Trust, London, 1969).
[40] W. B. Pearson, *A Handbook of Lattice Spacings and Structures of Metals and Alloys* (Pergamon, Oxford, 1967).
[41] L. Vegard, Z. Kristallogr. **89**, 560 (1934).
[42] B. B. Laird, J. Chem. Phys. **97**, 2699 (1992).
[43] K. J. Runge and G. V. Chester, Phys. Rev. A **36**, 4852 (1987).
[44] T. H. K. Barron and M. L. Klein, Proc. Phys. Soc. **85**, 4852 (1965).
[45] J. R. Neighbours and G. A. Alers, Phys. Rev. **111**, 707 (1958).
[46] S. Stølen and F. Grønvold, Thermochim. Acta **327**, 1 (1999).
[47] A. R. Denton and N. W. Ashcroft, Phys. Rev. A **43**, 3161 (1991).
[48] V. B. Warshavsky and X. Song, Phys. Rev. E **73**, 031110 (2006).